Solar Energy Materials and Solar Cells 184 (2018) 48–56

Contents lists available at ScienceDirect

Solar Energy Materials and Solar Cells

journal homepage: www.elsevier.com/locate/solmat

A four-state kinetic model for the carrier-induced degradation in multicrystalline silicon: Introducing the reservoir state

Tsun Hang Fung*, Moonyong Kim, Daniel Chen, Catherine E. Chan, Brett J. Hallam, Ran Chen, David N.R. Payne, Alison Ciesla, Stuart R. Wenham, Malcolm D. Abbott

School of Photovoltaic and Renewable Energy Engineering, University of New South Wales, Kensington, NSW 2052, Australia

ARTICLE INFO

Keywords:
Multicrystalline silicon
Carrier induced degradation
Kinetic state model
Defect reservoir
Hydrogen: Anneal

ABSTRACT

In this work, we present new insight into the multi-crystalline silicon carrier-induced defect (CID) by performing multiple degradation and regeneration cycles and further investigation on the partial recovery of mc-CID through extended dark annealing (DA). The maximum normalised defect density was found to decay exponentially with the number of cycles, suggesting that the defect precursors were slowly depleted by DA. A four-state kinetic model is proposed by introducing a reservoir state. Simulation results generated by mathematical modelling based on the proposed state diagrams exhibited good agreement with the experimental results. Extended DA on a partially recovered sample combined with simulation results suggests that the capability of defect formation through DA and the existence of the reservoir state proposed herein were the root causes for the partial recovery reported in the literature. Finally, the change in bound hydrogen state is speculated to cause the modulation of mc-CID formation. A qualitative reservoir model based on the interaction between hydrogen molecules (H_2), boron-hydrogen pairs (B-H) and free hydrogen (H^+, H°) is proposed and further discussed.

1. Introduction

Multi-crystalline silicon (mc-Si) degradation, occurring when mc-Si wafers are subject to illumination or current injection has been an increasingly researched area in the past few years [1–5]. Its importance has risen due to its impact on the Photovoltaics (PV) industry, with mc-Si PERC solar cells set to dominate the market within the coming decade [6]. The long periods of time required for the material to degrade and eventually recover within the field [4], compounded by the severity of degradation (up to 16% relative power loss [7]) results in a significant loss in total energy yield. Furthermore, it has recently been demonstrated that the same defect can also be found on solar grade Czochralski (Cz) wafers [8,9]. Degradation appears to occur regardless of which surface passivation method is used [4], which indicates a dependence on bulk-Si material. However, the responsible species and defect formation mechanism have not yet been identified. Since the degradation can be triggered by carrier injection either from illumination or bias voltage in the dark [10,11], the degradation will be referred to in this paper as multi-crystalline carrier-induced degradation (mc-CID) rather than light and elevated temperature induced degradation (LeTID), as it is often called [2]. Nevertheless, the occurrence of such degradation has also recently been reported in Cz silicon and Float-zone (FZ) silicon [8,12]. A more accurate terminology is required in the future.

Despite extensive research efforts in understanding mc-CID, as yet, no agreement on a kinetic state model has been reached. In contrast, a 3-state model which describes the kinetics of the BO meta-stable defect was established over a decade ago [13]. This model has greatly enhanced the understanding of the BO defect and has been referred to in numerous BO-related studies. In that 3-state model, defect precursors start at an initial state (state A) which is recombination-inactive and meta-stable. Under light soaking (LS), defect precursors transform into the degraded state (state B) which is recombination-active. Continued LS at elevated temperature then causes the recombination-active defects to transform into the regenerated state (state C), which is both recombination-inactive and stable at room temperature. However, the regenerated defect will transform back to the degraded state and subsequently to the initial state during dark annealing (DA) [14]. Some of these transitions are similar to what is observed in mc-CID; however that three state system is not able to explain all of the observed behaviours that have been reported.

Although mc-CID has a significantly longer time scale compared to BO related degradation, the behaviour under LS can be adequately described by the forward reaction in the 3-state model. For example, extensive LS causes the defect to become recombination-active and subsequently regenerate [2]. In addition, it has been shown that mc-CID

* Corresponding author.
E-mail address: tsun.fung@unsw.edu.au (T.H. Fung).

https://doi.org/10.1016/j.solmat.2018.04.024
Received 19 October 2017; Received in revised form 15 February 2018; Accepted 23 April 2018

defect formation and subsequent recovery could be accelerated by increasing temperature and/or excess charge carrier injection [10,15]. Recent studies suggest that the degradation rate constant of mc-CID at elevated temperatures possess a linearly-dependent relationship on excess charge carrier density with similar dependencies shown in BO formation rates at low illumination intensities [11,16]. Also similar to the BO system is the observation under some conditions of a two-step formation of the defect in which an initial fast degradation is followed by a slower one [17]. It has been further demonstrated that high intensity illumination can greatly accelerate the defect formation, a useful technique for studying the system given the long timescales required to complete a single cycle [10].

The response of the mc-CID system to annealing in the dark is more complicated than the BO system and remains less well understood. Early work demonstrated that the open-circuit voltage (V_{OC}) of pre-degraded mc-PERC cells was only partially recovered by dark annealing and furthermore that full regeneration was not achievable at a range of different temperatures [18]. In addition, the degradation rates under illumination after the partial recovery were found to be significantly higher than the initial degradation. Therefore, it was suggested that the state after annealing is different from the initial state before any degradation cycle and hence not fully reversible [18]. Nevertheless, in another study the dark annealing reaction was described as defect annealing in analogy to the BO defect model [15].

On regenerated samples, dark annealing was performed and injection dependent lifetime spectroscopy (IDLS) was used to analyse the defects responsible for each cycle [19]. Due to the significant difference in *k*-value extracted from the first and second cycle, it was suggested that different defects were activated by DA. Dark annealing prior to degradation was shown to greatly modulate the defect formation kinetics [20]. After applying DA at temperatures below 250 °C for 2.5 h, the degradation rate and severity of degradation was increased [20].

In contrast to the defect dissociation that occurs when dark annealing the BO-related defect, recent findings have shown that DA for mc-CID could in fact cause defect formation and subsequent recovery. This was demonstrated on mc-PERC cells where the V_{OC} degraded and then recovered under DA without illumination [20]. However, surface instability was not ruled out as a potential cause in that work. Subsequent studies confirmed that DA indeed caused the formation of the mc-CID defect, independent of any surface effects, with lifetime spectroscopy finding the *k*-value based on Shockley-Read-Hall (SRH) statistics [21] to be similar to the light-activated defect within the error range of the study [8]. As a result, it was suggested that DA could drive the forward reaction in mc-CID. Due to this distinct property, defect formation (forward reaction) and defect dissociation (reverse reaction) in analogy to the 3-state model could happen simultaneously under DA. If true then this should be accounted for when interpreting the defect annealing results previously reported within the literature [15,18].

A final key difference between the BO defect system and the mc-CID is the response to multiple cycles of formation and mitigation. The BO system is fully reversible, meaning that multiple cycles results in a similar amount of degradation with no change in the total amount of defects within the system [22]. However in the case of mc-CID, we have recently demonstrated that multiple cycles of degradation and regeneration cause a progressive reduction in the total amount of degradation [23]. Furthermore, the extent of degradation was related to the total thermal budget applied during dark annealing. This behaviour is difficult to explain within a 3 state system and it was proposed to include a fourth state [23]. Here we expand on this concept and provide further experimental data to demonstrate the validity (and limitations) of the four-state model for mc-CID.

We describe a defect kinetic state model that accounts for various observed behaviours of mc-CID. Experimental data and simulations results are presented to demonstrate the ability of the model to reproduce the trends in effective lifetime and normalised defect density in response to a variety of DA and LS conditions. The model requires many unknown inputs regarding the starting concentrations and rates of change. A detailed study of each would be required to accurately determine their values, and dependencies on carriers and on temperature. In this work we focus on the ability of the model to explain the broad trends and as such we calculate the inputs to the model by fitting the simulation results to the experimental data. In doing so we demonstrate that the behaviour of mc-CID can be explained by (1) the existence of a reservoir of state A precursors in the as-fired silicon, (2) a reverse reaction between the states other than the reservoir and (3) by a single recombination active defect. This final point is determined via lifetime spectroscopy of the experimental data. Subtle differences between the simulation and the experimental data are used to highlight areas for future improvement of the model and to provide insight into the root cause of the degradation. Finally, the implications of the model for the production of stable solar cells are discussed and an explanation for the kinetics based on the complex behaviour of hydrogen within silicon crystals is proposed.

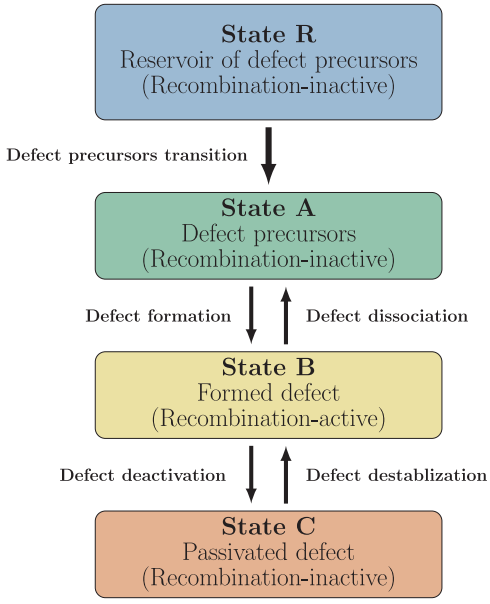

Fig. 1. Proposed four-state model for the mc-CID defect system. State A–C refer to the standard states in the original BO-LID model by Herguth et al. [13]. State R refers to the reservoir of state A precursors. Arrows represent transitions between the defect states.

2. Mc-CID state model

The four-state model used to describe mc-CID in this paper is shown in Fig. 1. States A–C are similar to the traditional 3-state model used to describe the BO defect [24]. In the mc-CID model, a reservoir of recombination inactive state A precursors (state R) is added prior to state A. Under dark or illuminated annealing conditions, state A precursors are released from state R into state A. In this paper, we assume this process is irreversible (or at least that any reverse reaction is insignificant for the investigated temperature regime). Furthermore, the inclusion of a reverse reaction from state A to R was not required to describe the experimental data presented herein. Such a state could represent for example an excess supply of a particular atomic species, created during the higher temperature processing followed by rapid cooling. The proposed model does not require illumination to drive any of the reactions forward [8], however any of the transitions could be accelerated by the introduction of excess carrier injection. Finally, small but non-negligible reverse reactions have been included which allows transition from state C back to state A through state B.

In this paper we chose to simplify the degradation step to a single state transition (A→B), rather than the two step degradation reported in

the literature [17]. Future refinements of the model could expand state A into a double step (A1 and A2) similar to a recent modification proposed for the BO-LID state diagram [25]. This simplification is valid for the modelling within this paper since we choose processing conditions for which the impact of two-step degradation would be negligible. In doing so the number of free input variables that are required to fit to the experimental data is reduced. It is worth noting that state R presented herein is different to a state A1 where the population of state A1 affects the extent of fast and slow degradation within one cycle [26] while the population of state R affects the decrease in degradation extent through multiple cycles.

The concentration of defects or precursors in each of the states ($N_i(t)$), where i = R, A, B, C, are governed by a system of linear differential equations given by Eqs. (1)–(4). Here, k_{ij} is the rate constant from state i to j.

$$\frac{\partial N_R}{\partial t} = -\kappa_{RA} N_R \tag{1}$$

$$\frac{\partial N_A}{\partial t} = \kappa_{RA} N_R + \kappa_{BA} N_B - \kappa_{AB} N_A \tag{2}$$

$$\frac{\partial N_B}{\partial t} = \kappa_{AB} N_A + \kappa_{CB} N_C - \kappa_{BC} N_B - \kappa_{BA} N_B \tag{3}$$

$$\frac{\partial N_C}{\partial t} = \kappa_{BC} N_B - \kappa_{CB} N_C \tag{4}$$

A boundary condition for the defect concentration is included, such that the sum of all population equals to unity at any processing stages. This represents a conservation of defect components in the proposed four-state system. In this work the values of the rate constants for the above equations have been determined via fitting the experimental data and through a series of assumptions. This is necessary due to the current lack of reference materials in the literature regarding the exact rates. While this may at first seem somewhat arbitrary given the large number of inputs, it is worth noting that many of the behaviours cannot be explained outside of the four-state model. This will be demonstrated through the following experiments. Future work should investigate these reaction rates in more detail, including a study of the impact of temperature and carrier injection.

3. Experimental

1.3 Ω cm p-type boron-doped high performance (HP) multi-crystalline wafers, selected from neighbouring locations in the ingot, were used to fabricate symmetrical lifetime structures. Wafers underwent acidic texturing to a final thickness of about 180 µm. A phosphorus diffusion was performed on all wafers in a $POCl_3$ tube furnace resulting in ~70 Ω/□ emitter on both sides. Hydrogenated silicon nitride (SiN_X:H) dielectric layers with a thickness on 75 nm and a refractive index of 2.08 (at 633 nm) were deposited on both sides using a Meyer Burger MAiA remote plasma-enhanced chemical vapour deposition tool [27]. Wafers were fired with peak wafer temperature of 740 °C at a constant belt speed of 4.5 m/s, in a Schmid fast-firing metallization belt furnace. Wafers were laser cleaved into tokens (39 mm × 39 mm) and grouped to form "sister" sets with similar crystallographic grain patterns originating from their close proximity within the ingot.

The samples were then split into two groups; the first was used to demonstrate the existence of state R and to provide evidence for the reverse reaction. The second was used to demonstrate how the state diagram can explain the partial recovery reported by Luka et al. [18]. In the first experiment, a sample was cycled through a process of: (1) DA at 232 °C for 8 mins, (2) LS at 135 °C with illumination intensity at 25.7 kW/m^2 to form defects and recover. These processes were repeated for nine cycles with the same DA and LS conditions. In the second experiment, a sample was LS at 45 kW/m^2 and 138 °C. The lifetime was monitored between each short illumination process until a minimum and hence the fully degraded state was achieved. DA at 175 °C was then applied; the lower temperature was used to slow down the lifetime recovery such that more clear time intervals can be shown. A control sample underwent the same DA condition without being subjected to LS after firing. The effective lifetimes after firing were used as initial values for calculating normalised defect density (NDD) for both samples. In both experiments the effective lifetime was monitored throughout the processing.

For all LS processes, the sample was placed on a hotplate with vacuum to ensure good thermal contact during LS and the temperature variation was monitored by an external infra-red sensor. The illumination was supplied by a 938 nm laser and the intensity was controlled by adjusting laser current. A homogenizer lens was used to achieve uniform laser intensity across the wafer surface with variation less than 5%. The illumination duration was computer-controlled to minimise processing error between samples. The temperature of the sample during illumination was monitored by a calibrated infra-red sensor. The sample reached the desired operating temperature within 1 s. However, due to the high intensity illumination provided by the laser, the temperature of the sample gradually increased during each laser illumination. This resulted in a fluctuation in temperature of ± 2 °C and ± 3 °C during degradation and regeneration respectively. Generally, the fluctuation increased with increasing illumination duration. The DA processes were performed by placing the samples on the same hotplate with the laser turned off.

The effective minority carrier lifetime was measured by quasi-steady-state photo-conductance via the generalised technique using Sinton WCT-120 [28,29]. Auger recombination was corrected by using the Richter model [30]. The NDD was calculated by using the following equation:

$$NDD(t) = \frac{1}{\tau_{\mathrm{eff(t)}}} - \frac{1}{\tau_{\mathrm{eff(0)}}}$$

where $\tau_{\mathrm{eff(t)}}$ and $\tau_{\mathrm{eff(0)}}$ is the effective lifetime measured at any given time and initial state respectively. Note that in the first experiment the value for $\tau_{\mathrm{eff(0)}}$ was taken from the lifetime measured after DA for each cycle. This accounted for a gradually improving background lifetime during the cycling process.

The injection-dependent SRH properties of the mc-CID defect were analysed by lifetime curve fitting and minimising the goodness-of-fit. Chi-square of the fitted curve was used to determine error bars [31]. The initial effective lifetime curve was fitted with the equation below:

$$\frac{1}{\tau_{\mathrm{eff(0)}}} = \frac{1}{\tau_{\mathrm{bulk}}} + \frac{1}{\tau_{\mathrm{surface(0)}}} + \frac{1}{\tau_{\mathrm{SRH\_background}}}$$

where τ_{bulk} is the injection-independent bulk lifetime component, $\tau_{\mathrm{surface(0)}}$ is the initial surface recombination related lifetime component and $\tau_{\mathrm{SRH\_background}}$ is the SRH recombination related component occurring in the background before inducing mc-CID, caused for example by other metal impurities and crystallographic defects. The mc-CID activated effective lifetime curve was fitted by fixing the $\tau_{\mathrm{SRH\_background}}$ and τ_{bulk}, floating the surface component and incorporating an additional SRH component ($\tau_{\mathrm{SRH\_CID}}$):

$$\frac{1}{\tau_{\mathrm{eff(t)}}} = \frac{1}{\tau_{\mathrm{bulk}}} + \frac{1}{\tau_{\mathrm{surface(t)}}} + \frac{1}{\tau_{\mathrm{SRH\_background}}} + \frac{1}{\tau_{\mathrm{SRH\_CID}}}$$

The energy level of the $\tau_{\mathrm{SRH\_background}}$ and $\tau_{\mathrm{SRH\_CID}}$ were both assumed to be at mid-gap. Note that allowing the surface lifetime component to change during the activation of the mc-CID is important since it has previously been shown to have the potential to vary [31,32] and this can have a significant impact on the subsequent curve fitting. Previous work that studied curve fitting to lifetime curves of metastable defects found that allowing the surface component to float reduced the Chi-square and median absolute deviation while floating both surface component and τ_{bulk} could potentially result in "over-fitting" due to large degree of freedom [31]. The change in surface

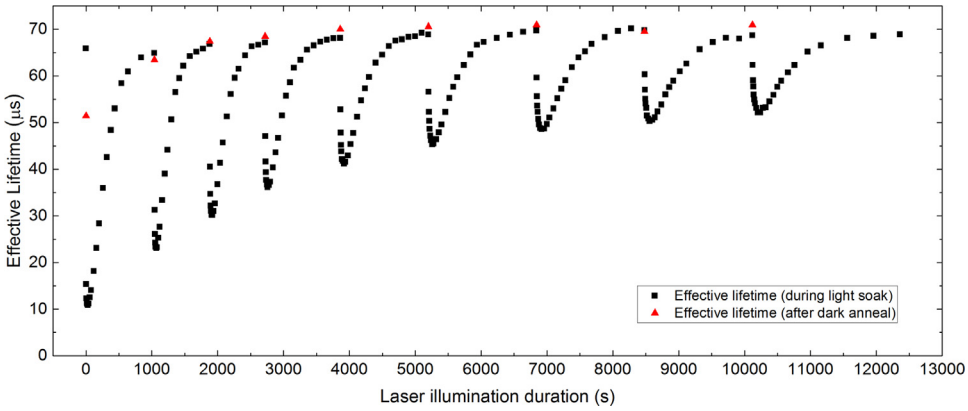

Fig. 2. Effective minority carrier lifetime extracted at 9.1 × 10^{14} cm^{-3} injection level as a function of time when processed with 25.7 kW/m^2 illumination at 135 °C. The lifetime was monitored incrementally during illuminated processing (black squares) and measured after a dark annealing process for 8 min at 232 °C (red triangles).

recombination current density (J_{0e}) in this study was found to be more profound in the first cycle (~ 20 fA/cm^2) than latter cycles (~ 5 fA/cm^2). Further information regarding the fitting approach adopted in this study could be found in "method D" in Nampalli et al. [31].

4. Results and discussion

4.1. Impact of dark annealing and light soaking cycles

The evolution of effective lifetime through a series of DA-LS cycles (Fig. 2) demonstrates the changing amount of meta-stable defects within the system under these process conditions. The evolution of effective lifetime during the accelerated light soak process (Fig. 2 black squares) shows the formation and subsequent removal of the defect for each cycle. If the LS process conditions were continued then the lifetime would remain stable and recovered. However, the application of a DA process (at a higher temperature) at the end of the cycle (Fig. 2 red triangles) caused the system to once more become unstable. After the first DA process, the effective lifetime reduced from 65 μs to 51 μs. Subsequent LS resulted in a minimum at 10 μs during the first cycle. After reaching a regenerated state, a second dark anneal was applied and resulted in a reduced minimum at 23 μs in the second cycle. As the cycle was repeated, the extent of degradation was found to progressively reduce, finally reaching a minimum lifetime of 52 μs during the ninth cycle. This reduction in total degradation with each cycle is fundamentally different to what is typically observed for BO or Fe_i instabilities in silicon.

The effective lifetime after each regeneration cycle was observed to progressively increase. This is likely due to the passivation of other defects under laser illumination (possibly via interaction with hydrogen). This difference in DA effective lifetime from the third cycle to the ninth cycle was about 4 μs (from 67 μs to 70 μs), which is relatively small compared to the reduced effective lifetime at degraded state (30–52 μs). It was assumed that the passivation of other non-LeTID related defects under illumination mainly occurred during the long regeneration process (< 1000 s) or during DA. However, such changes to the background lifetime are important to consider during curve fitting of injection level dependent lifetime data. Therefore, the DA lifetime curve prior to each cycle and the degraded lifetime curve in the corresponding cycle were used to calculate NDD and fitting of SRH defect statistics. The illumination duration required to fully degrade the sample was rather short (< 20 s). As a result, the increase in bulk lifetime should have minimal effect on both NDD calculation and SRH fitting.

To more easily interpret the experimental data as a CID bulk defect the effective lifetime was converted into a normalised defect density. Plotting this as a function of laser illumination time (Fig. 3a) reveals how the total amount of the defect changes during the process cycles. It has to be noted that negative values of NDD toward the end of the first

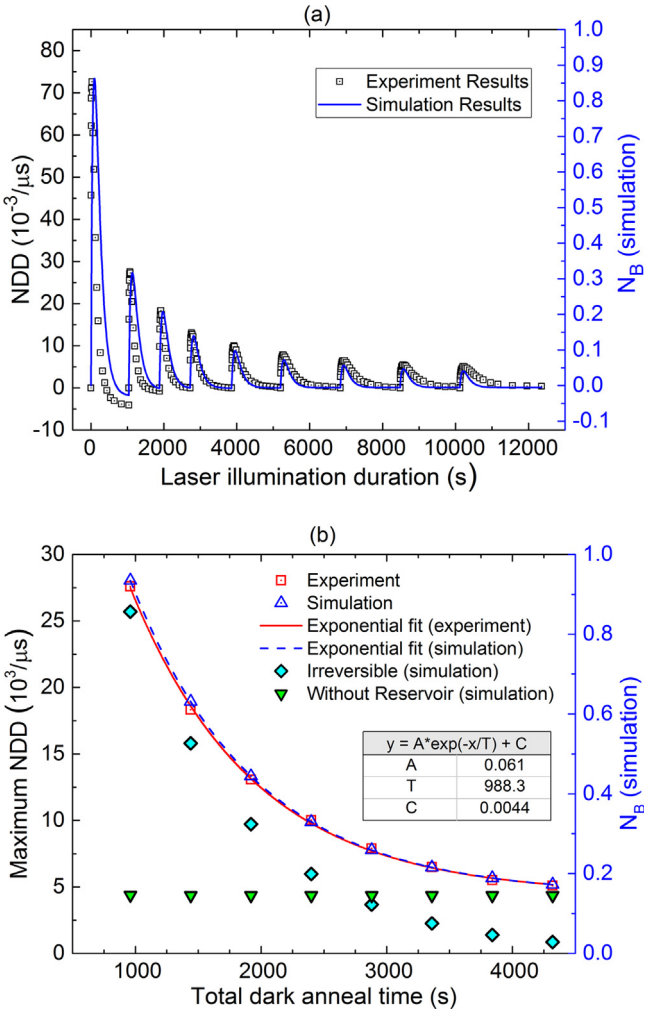

Fig. 3. (a) Evolution of NDD during DA-LS cycles (black squares) and simulation results of N_B during DA–LS cycles based on the proposed four-state model (blue line). **(b)** Maximum NDD with total DA time (red squares). Simulation results of maximum N_B with total DA time based on: the four state model (blue triangles), the four state model without reverse reactions (cyan diamonds) and the three-state model (green inverted triangles) with no reservoir. The inserted table lists the parameters resulted from fitting of experimental data (red line).

cycle were observed. The reason for the negative values is because DA in the first cycle caused partial degradation prior LS. Therefore, subsequent LS caused the lifetime regenerated over the DA lifetime in the first cycle. The maximum amount of NDD can also be plotted as a function of the total amount of DA time that has been applied to the

Table 1
Rate constants used in simulation of the transition of defect population under DA-LS cycles based on the proposed four-state model.

	LS at 25.7 kW/m^2 and 135 °C (/s)	DA at 232 °C for 8 min (/s)
k_{RA}	0	1.02×10^{-3}
k_{AR}	0	0
k_{AB}	1.5×10^{-2}	2.46×10^{-4}
k_{BA}	1.5×10^{-4}	7.26×10^{-3}
k_{BC}	6.75×10^{-3}	2.46×10^{-3}
k_{CB}	3.38×10^{-5}	6.05×10^{-5}

system (Fig. 3b). In this case a clear exponential decay is observed which can be fit using the equation shown in the figure. Note that the exception to this is the NDD_{max} at t_i = 480 s (not shown in figure, NDD_{ti} = 0.073/μs) which had significantly more defects due to the introduction of defects during the firing process. In the four-state model the NDD is analogous to the concentration in State B. On both charts, the curve-fit resulting from the simulation is plotted on secondary y-axis.

The four-state model was able to achieve a reasonable fit to the experimental data. This was done by setting the initial concentrations (N_R = 0.76, N_A = 0.23) and using the rates shown in Table 1. The values were determined using an iterative process of setting the concentration and adjusting the rates. The values of N_R and N_A were obtained by changing the ratio to get a good fit of the NDD_{max} of the first and second cycle. The rate of release of defect precursors into the system (k_{RA}) was set to match the decay constant of the exponential fit of NDD_{max} under DA conditions. The rate constant for the reverse reaction (k_{CB} and k_{BA}) under DA was obtained by fitting the saturation level of the NDD_{max} during cycling. The defect formation and de-activation rate under LS was chosen to give a LS cycle under similar timescale to the actual data and in such a way as to leave N_A as zero at the end of the cycle.

To demonstrate the necessity of the reservoir and of the reverse reactions, further simulations were performed firstly with the values of all reverse rates set to zero (Fig. 3b cyan diamonds) or secondly with no state R, but reverse reactions enabled (Fig. 3b green inverted triangles). In the first case the maximum NDD approaches zero since there is no introduction of new defects and inevitably the system is driven into state C. In the second case the maximum NDD is the same for each cycle, since the total population of defects in the 3-state system is not changing and the DA acts to reverse the same amount of defects from state C back to state A prior to each LS cycle.

The results presented above support the hypothesis that the behaviour of the mc-CID during this cycling experiment could be described via the existence of a reservoir of state A precursors. The contents of this reservoir are gradually reduced during the dark annealing conditions but not significantly so during the rapid light soak process at a lower temperature. Furthermore once the reservoir is depleted, the mc-CID defect system reaches a steady state concentration of the defects which are then cycled back and forth (similar to the BO defect system). This scenario is illustrated in Fig. 4a which shows the concentration in each of the states predicted by the simulation of the DA-LS cycles. Since k_{RA} is relatively large compared to k_{AB} under DA (232 °C), the reservoir is depleting and it causes an accumulation in N_A prior to LS. Under LS (135 °C), k_{RA} is assumed not to be accelerated by excess carrier injection. Therefore, N_R stays relatively constant while the defect precursors are transitioning from state A to state B then to state C. N_R is eventually depleted through cycling as a result of an irreversible transition between state R and state A (Fig. 4b). After N_R is depleted, DA causes a fixed amount of defect precursors to transit from state C back to state A as a result of reverse reaction between state A, B and C. Consequently, DA causes the same amount of N_B to form in subsequent cycles.

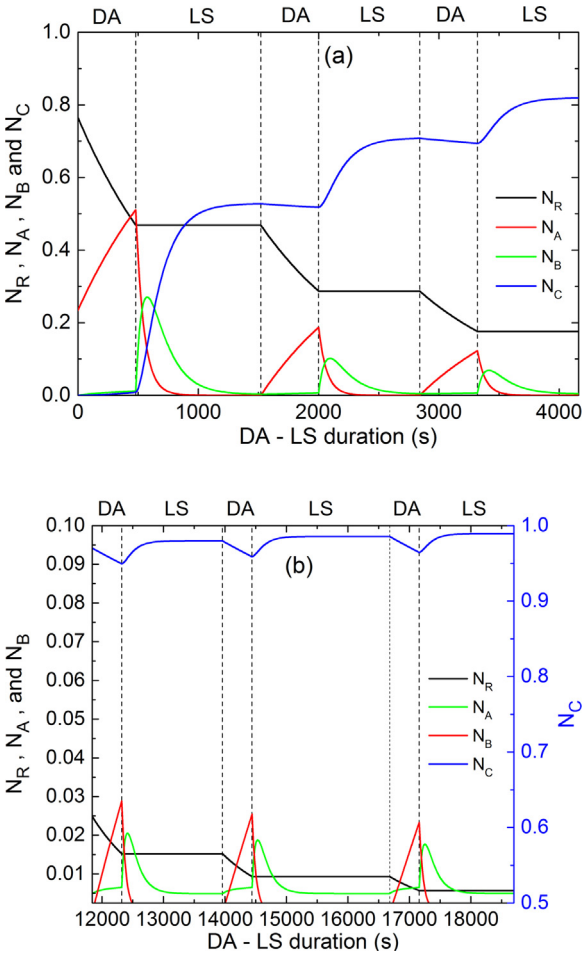

Fig. 4. Simulation results of the evolution of N_R (black), N_A (red), N_B (green) and N_C (blue) during **(a)** early cycles and **(b)** later cycles based on the proposed four-state model.

4.2. Incomplete recovery of lifetime with dark annealing

One of the interesting observations in the literature that has been difficult to explain with a simple state diagram and a single defect is the occurrence of an incomplete recovery of lifetime during DA [18]. This scenario was reproduced in the second experiment by comparing the response to dark annealing of an as-fired sample (Fig. 5, red triangles) and a sample degraded after firing (Fig. 5, blue squares). The NDD of the pre-degraded sample started at 1.7×10^{-2}/μs before decreasing to 2.3×10^{-3}/μs after 600 s DA. From there it then increased again to a second peak at 1.1×10^{-2}/μs after 24,000 s. The NDD of an as-fired sample increases with DA duration until reaching a peak at 1.2×10^{-2}/μs after 18,000 s before both samples decay down to sub-zero values.

The experimental data presented in Fig. 5 is consistent with the results presented by Luka et al. where it was suggested that the defect is in a different state to the initial state after annealing and that the defect formation is not totally reversible [18]. However, the possibility of driving the forward reaction by DA and the potential existence of a reservoir of state A precursors were not considered in that study. Within the four-state model, the partial recovery of lifetime can be explained by a competition between defect formation and defect de-activation. After light soaking, some population of defects is in the degraded state. When DA is applied, the transition toward de-activation is dominant in the early stages of annealing, thus the NDD is decreasing. As DA continues, extra defect precursors are released from the reservoir and slowly form recombination active defects. A plateau in lifetime

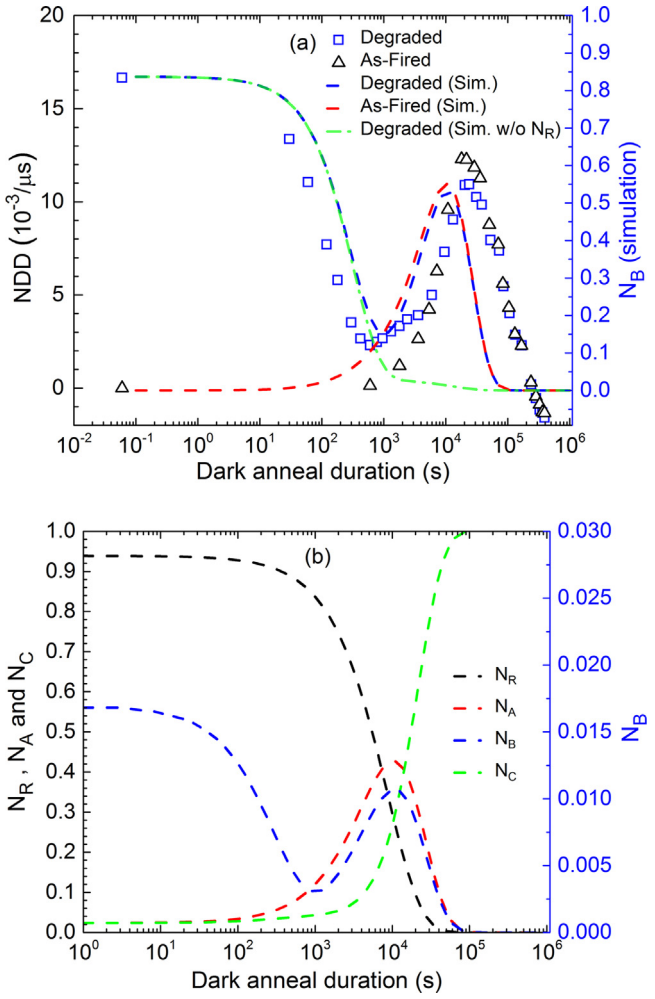

Fig. 5. (a) Evolution of NDD with DA for a laser degraded sample (blue labels) and as-fired sample (red labels). Simulation results of N_B during DA based on the proposed four-state model for pre-degraded state (blue line), as-fired state (red line) and pre-degraded state without reservoir (green line). **(b)** Simulation results of N_R (black line), N_A (red line), N_B (blue line) and N_C (green line) during DA based on the proposed four-state model for pre-degraded state.

recovery is reached when the transition of defect formation is comparable to the defect de-activation. After reaching the partial recovery, extended dark annealing caused the transition of defect formation to dominate. Hence, the NDD is temporarily increased reaching a second degraded state before finally the defects from the reservoir are depleted and again the lifetime recovers. With this explanation, a single defect is responsible for the partial recovery from the light soaked state by DA. It must be noted that subsequent degradation under DA after partial recovery was not observed in the study by Luka et al. [18]. This could be due to shorter DA duration (200 °C for 25 min and 150 °C for 200 min) compared to the duration required to achieve second degraded state in the results presented herein (175 °C for 400 min).

Again the four-state model presented in Section 2 was able to reproduce the trends in the experimental data. This was done by setting the initial concentrations (N_R = 0.93, sum of $N_{A,B,C}$ = 0.07) and using the rates shown in Table 2. The values were again determined using an iterative process. The values of N_R and sum of $N_{A,B,C}$ were obtained by increasing the ratio used in DA-LS cycling until the second peak appeared. The rate of defect de-activation was first adjusted to fit the recovery from LS state (before 10^3 s). The rate of release of defect precursors into the system (k_{RA}) and the rate of defect formation (k_{AB}) were adjusted to fit the degradation after achieving partial recovery (between 10^3 s and 10^4 s) by keeping $k_{RA} > k_{AB}$. Finally, all the rate

Table 2
Rate constants used in simulation of the transition of defect population under DA at as-fired state and LS-state based on the proposed four-state model.

	DA at 175 °C (s^{-1})
k_{RA}	1.15×10^{-4}
k_{AR}	0
k_{AB}	7.68×10^{-5}
k_{BA}	0
k_{BC}	3.10×10^{-3}
k_{CB}	0

constants were re-adjusted to give the best fit overall. The reverse reactions were excluded to reduce the number of fitting parameters as they are not necessarily required to reproduce the partial recovery. It can be observed that the minima of the simulation result occurred later compared to the experimental data while the maxima occurred earlier. This could be due to the use of an incorrect rate constant and initial population in the simulation. However, the simulation adequately demonstrated the key features of the curve which N_B initially reached a partial recovery then followed by an increase until reaching the second maxima.

Fig. 5(b) shows the simulated results for the transitioning of defect precursors during DA for the pre-degraded case. N_B decreases as a result of transition from state B to C. In the meantime, defect precursors transit from the reservoir to state A. Since N_R is much larger than N_A and k_{AB} is smaller than k_{RA}, it causes defect precursors to accumulate in state A. Hence, N_A increases significantly. As DA is continued, the transition of defect precursors from state A to B becomes increasingly significant which causes N_B to increases. Finally, N_B decreases toward zero as a result of transition from state B to C.

It is worth noting that in both experiments (Figs. 2, 3 and 5) there was a slight discrepancy between the simulation and experimental data regarding the rates of formation and mitigation over time. For example, from looking closely at Fig. 3(a) it can be seen that initially the simulation under-estimates the rate and in the later cycles over estimates them. Similarly the final rate of mitigation shown in Fig. 5 is not perfectly matched to the simulation result. The underlying reason for this is that in the experimental data the actual rates appear to change, beyond what would be expected due to overall changes in the starting concentrations. This may suggest that further refinement of the model is necessary to account for these changing rates. For example it may be that the rate is somehow related to the total population of the defects in the system. Alternatively this could be related to the use here of a single formation rate between states A and B rather than a fast and a slow rate predicted in the recent findings by Bredemeier et al. [17]. It should also be pointed out that the set of rate constants used in the second simulation should be smaller than the set used in the first simulation, due to the fact that a lower DA temperature was used. However, k_{BC} was found to be larger in the second simulation while the rest of the parameters (k_{RA} and k_{AB}) seemed reasonable. The discrepancy could be caused by the simplifications used in the second simulation (e.g excluding reverse reactions between State A, B and C). Moreover, including a sub-state between state A and state B, as suggested above, might be able to fix the problem in future investigations. Finally, the known injection dependency of mc-CID degradation rate was neglected in the simulation. This assumption is considered valid in this work due to the fact that carrier injection was done by using high intensity laser (~ 25 suns), such that the lifetime sample was operating at extremely high injection level (well beyond 1×10^{16} cm^{-3}). As a result, the effective lifetime tends to be limited by Auger recombination and surface recombination and therefore has almost no difference in either the degraded or initial state during the accelerated defect formation process itself. However, the final model should include this injection dependency for a more general application (~ 1 sun).

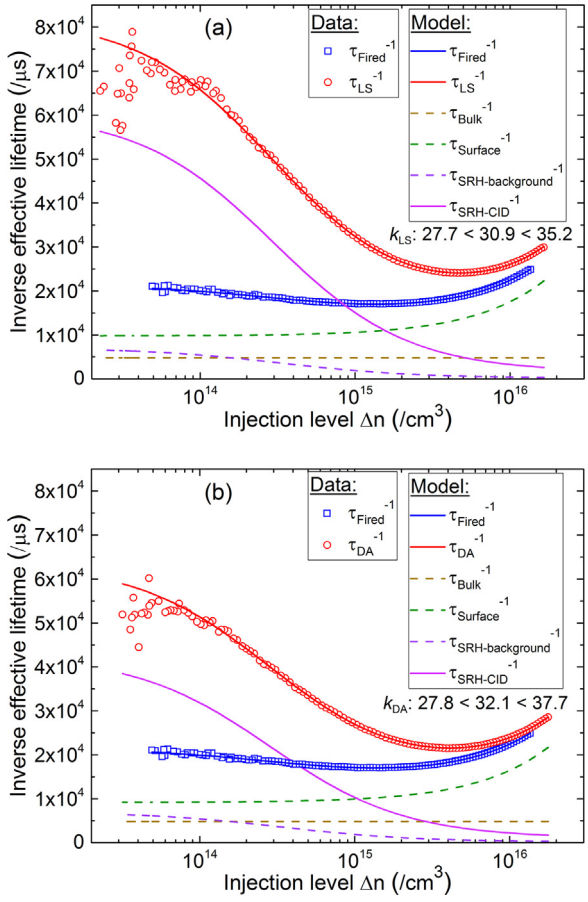

Fig. 6. IDLS data showing measured injection dependent inverse minority carrier lifetime for **(a)** Laser degraded state and **(b)** DA degraded state after reaching partial recovery. The as-fired lifetime and degraded lifetime are shown in blue square and red circle respectively. The fitted lifetime components are indicated by the coloured lines: τ_{fired}^{-1} (blue), $\tau_{degraded}^{-1}$ (red), $\tau_{SRH\_CID}^{-1}$ (solid purple), $\tau_{SRH\_background}^{-1}$ (dash purple), $\tau_{surface}^{-1}$ (green) and τ_{bulk}^{-1} (orange).

4.3. SRH analysis of defects induced by DA and LS

One of the features of the four-state model proposed here is that a single defect is responsible for the degradation of the lifetime. To provide some insight into this, injection-level dependent lifetime analysis was performed to reveal more information about the defect responsible for the observed degradation and recovery. Curve fitting at the degraded state achieved by laser illumination prior to DA (Fig. 6a, corresponds to initial blue square in Fig. 5a) and the DA degraded state following the partial recovery (Fig. 6b, corresponds to blue square at 20,400 s in Fig. 5a) indicates very similar SRH properties. The as-fired state was used as the initial effective lifetime curve for both cases. For the degraded state caused by laser illumination, the *k*-value was found to be between 27.7 and 35.2. For the degraded state caused by DA after achieving partial recovery, the *k*-value was between 27.8 and 37.7. Since the extracted *k*-values for both states lie within the errors of each other, there is no evidence to indicate that these are different defects. Hence, a single defect could be responsible for the partial recovery from LS state, as a result of the forward reaction caused by DA.

Similar analysis was performed throughout the cycling experiment from Fig. 3. For each cycle, the lifetime curve in the degraded state was compared to the lifetime curve after DA for that cycle. The extracted *k*-value for each cycle (Fig. 7) was found to lie within the error bars for all subsequent cycles. A slightly increasing trend in both the optimal *k*-value and the error bars was observed with the increasing number of

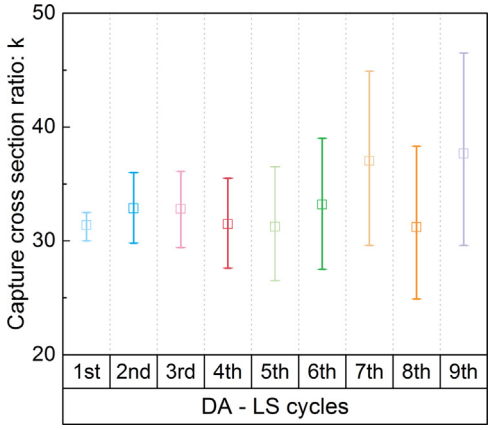

Fig. 7. The extracted capture cross-section ratio in each cycle with error bar during DA-LS cycling experiment.

cycles. A possible explanation for this is the increasing impact of the background lifetime on the curve fitting as the total influence of the mc-CID is reduced. The *k*-values extracted in this work agree with Morishige et al. who found *k*-value between 26 and 36 [33]. It also agrees with Niewelt et al. who found k-value about 35 ± 10 in light-activated defects in float-zone silicon [12]. Overall, the SRH introduced by the defect formation process can be explained by a single defect and there is no evidence to support claims that a different defect was responsible for the decay and the saturation in NDD_{max} observed.

This finding appears to contradict the results from Jensen et al. in which it was suggested that the defect activated in the second LS cycle is different from the one activated in the first cycle when DA is applied after the first complete regeneration [19]. That work's conclusion was based on the significantly different *k*-values extracted in the different cycles. A possible cause for this discrepancy could be the differences in the assumptions used in the analysis of the lifetime curves. For example, that work assumed no changes in surface lifetime, which are accounted for in the result above. In addition, the lifetime samples used in that work have no emitter on the surface, which might cause the effective lifetime to be more sensitive to degradation of surface passivation [32]. It is also impossible to compare exactly the lifetime response of different wafers from different sources in which numerous other defects may or may not be present.

4.4. Implications of the four-state model and speculation on the degradation mechanism

The proposed four-state model, and in particular the existence of the reservoir, has some important implications for the study and mitigation of mc-CID. If the creation of defects from state R is insignificant for normal solar cell operation then post process mitigation strategies need only focus on moving defects from state A into C. In this case, the time spent at elevated temperature during the cooling zone of the fast firing process and in the laminator become important as they allow defect precursors to be released from R. Certainly any mitigation strategy employed prior to lamination that does not fully deplete state R is unlikely to result in modules that are fully stable. It is also important to consider state R when studying the kinetics of mc-CID since it may be modulating the total number of defects within the A, B, C system.

The details of the four-state diagram also provide some insight into the underlying cause of the degradation and the chemical species that drives the kinetics. In particular the inclusion of State R, a supply of defect precursors that is depleted over time, provides clues. Combined with the knowledge that high temperature firing is required to initiate the meta-stable defect [34,35] a possible explanation for the precursors in state R is a defect species, formed during the high temperature firing process, that is then present in the bulk in concentrations higher than

what thermal equilibrium predicts during the subsequent lower temperature process conditions. Two likely candidates for this are species of vacancies and/or hydrogen, both of which are introduced into the silicon at the higher temperatures and when subject to quenching could exist in numerous configurations outside of that required by thermal equilibrium. Certainly hydrogen has been identified numerous times as likely to be involved in mc-CID [19,20,34,36] and more recently vacancies have also been proposed to be possibly involved [37]. During high temperature firing, hydrogen is introduced throughout the bulk of the silicon and is present in atomic form [38]. As the silicon is rapidly cooled (quenched), the solid solubility of interstitial hydrogen in silicon decreases and a large fraction of the atomic hydrogen either bonds with impurities and defects (passivating them), is aggregated to hydrogen molecules (H_2) [39,40] or is trapped by boron, forming boron-hydrogen pairs (B-H). If interstitial hydrogen is one of the mc-CID precursors (or is in fact the defect itself [41]) then changing the bound state of hydrogen is expected to affect the kinetics of mc-CID.

Subsequent to fast-firing, the majority of hydrogen exists in molecular form (H_{2A}) leaving only a small fraction of B-H [38]. This molecular hydrogen could explain the state R within the four-state model. During dark annealing, H_{2A} dissociates to H^+ and H° through a hole-assisted reaction ($H_{2A} + h^+ \rightarrow H^+ + H^\circ$) [38]. The H^+ will then be trapped by B^- to form B-H pairs, resulting in an increase in the concentration of B-H that would be very temperature-dependent. This B-H could be state A; non-recombination active but ready to supply defect precursors (interstitial H) during future processing. The dissociation of B-H pairs in the dark is strongly inhibited due to the coulombic attraction between H^+ and B^-. However, carrier injection (e.g. illumination) reduces the activation energy for dissociating B-H from 1.76 ± 0.05 eV to 1.1 ± 0.1 eV [42] (comparable to the reported mc-CID slow degradation rate: 0.94 ± 0.06 eV [17]). One possible mechanism suggested for this was a change in the charge state of hydrogen from H^+ to H° thus allowing it to more easily to escape from B^- after dissociation [43]. Consequently, the H° that escaped could then diffuse and reach another species to cause the recombination-active defect under illumination (state B). Extended dark annealing (particularly at higher temperatures) will cause the concentration of B-H (and H^+) to decrease due to formation of H_{2C} [38]. This molecule is considered to be more stable than H_{2A} and possibly represents a more stable bulk lifetime for the silicon wafers. If this physical explanation for the four-state model is correct, then it would also mean that state R provides species for both state A and state B. The implications of this should be studied in further development of the model.

The role of the different hydrogen species and their response to temperature and illumination potentially explains some other observations within the literature. Previously, it was reported that the mc-CID defect formation rate was accelerated by low temperature DA but decelerated by high temperature DA [20]. If B-H indeed acts as a precursor state for mc-CID, the modulation of the rate of defect formation could be explained by the change in [B-H] as a result of DA [44]. It might also explain the reduced defect formation rate in the later cycles after multiple DA steps presented herein (B-H concentration decreases). The generation of H° through dissociation of H_{2A} under dark annealing might also explain the recent results which suggests that dark annealing causes the same recombination-active defect as illumination [8]. It has also been shown that grain boundaries in undoped polycrystalline silicon act as an efficient hydrogen trap rather than a path of enhanced diffusion [45]. Therefore, the presence of such grain boundaries is likely to reduce the concentration of B-H in those regions. Consequently, the involvement of B-H in mc-CID also fits into the results presented by Luka et al., who demonstrated that the defect density of mc-CID was reduced in the regions of grain boundary [46]. Another defect model presented by Bredemeier et al. proposed that an interstitial metal atom (M_i) captured a uniformly distributed impurity (X) during rapid cooling and formed a metal complex (M_i-X) [34]. Under LS, M_i-X reconfigured to a more recombination active form M_i-X^* (resulting into fast degradation) and then slowly dissociate to release highly recombination active M_i (resulting into slow degradation). As a result, the fast and slow degradation could be resulted by two different species, which might differ to the single-defect mechanism proposed herein. Future investigation on the *k*-value extracted at different stages of degradation should reveal more information regarding this issue. The existence of a reservoir demonstrated herein was ascribed to the formation of B-H and H_2. However, such reservoir might also be described in the context of models proposed by Bredemeier et al. where the precipitation form of M_i dissociates under DA with hydrogen playing the role of the uniformly distributed impurity. Recent results from Bredemeier et al. have also suggested that the wafer surface acts a path to remove the defect over longer periods of time [47]. A hydrogen based model could similarly be expanded to include a loss of hydrogen from the wafer surfaces. Such a model would likely be heavily impacted by the presence of surface diffusions and as such should be validated in the near future. The importance of B-H has previously been demonstrated for the BO defect. In studies of the BO related defect where hydrogen plays a role in regeneration, it was shown that modulation of the B-H concentration (via dark annealing) changed the regeneration rate [48]. It was suggested that DA modulates the bound state of H (concentration of B-H) and hence the concentration of mobile hydrogen during regeneration. In mc-CID where hydrogen might play a role in defect formation, the mobile hydrogen might act as precursor for the defect formation reactions through the release of hydrogen from B-H which is also carrier-accelerated. Therefore, the concentration of B-H could modulate mc-CID degradation rate.

5. Conclusion

In this study, a four-state kinetic model including a reservoir state was proposed in describing mc-CID. The existence of the reservoir state and reverse reactions were supported by the decay and saturation of NDD_{max} through multiple DA-LS cycles. The partial recovery by DA from the LS state reported in literature was further investigated; the capability of defect formation by DA and the existence of the reservoir state proposed herein were suggested as the root causes. SRH analysis suggested that a single defect could be responsible for the observed behaviour.

Simulated results based on the four-state model exhibit good agreement with the experimental data. In particular, the decay and saturation of NDD_{max}, and the key feature of partial recovery and subsequent degradation under DA, were captured by the modelling. Nevertheless, the actual rate constants between each state, initial population conditions and further refinement of the model are required to improve the quality of fit.

Finally, changes in bound hydrogen states were speculated to cause the modulation of mc-CID formation rate. A qualitative reservoir model based on the interaction between H_2, B-H, H^+ and H° was proposed and further discussed. The H° generated by dissociation of H_2 was suspected to cause mc-CID formation under dark annealing. The change in concentration of B-H was suspected to cause the modulation of degradation rate by dark annealing prior light soaking. The H° generated by dissociation of B-H under minority carrier injection was suspected to cause accelerated formation of mc-CID under illumination. Nevertheless, hydrogen could have different bonding-states in silicon other than the B-H discussed herein (e.g. V_nH_m, CH, OH) that could still fit with the four-state model proposed. The possibility that other hydrogen bonding states play a role in mc-CID will be investigated in the future.

Acknowledgments

The authors would like to thank Duc Huy Dao, Ly Mai who assisted with sample processing. This work was supported by the Australian Government through the Australian Renewable Energy Agency (ARENA: 1-A060), the Australian Centre for Advanced Photovoltaics

(ACAP: funding for facilities). Responsibility for the views, information, or advice expressed herein is not accepted by the Australian Government. The authors would also like to thank the commercial partners of the ARENA 1-A060 advanced hydrogenation project.

References

[1] J. Lindroos, Y. Boulfrad, M. Yli-Koski, H. Savin, Preventing light-induced degradation in multicrystalline silicon, J. Appl. Phys. 115 (2014), http://dx.doi.org/10.1063/1.4871404.

[2] F. Kersten, P. Engelhart, H. Ploigt, A. Stekolnikov, T. Lindner, F. Stenzel, M. Bartzsch, A. Szpeth, K. Petter, J. Heitmann, J.W. Müller, Degradation of multicrystalline silicon solar cells and modules after illumination at elevated temperature, Sol. Energy Mater. Sol. Cells 142 (2015) 83–86, http://dx.doi.org/10.1016/j.solmat.2015.06.015.

[3] K. Krauss, F. Fertig, D. Menzel, S. Rein, Light-induced degradation of silicon solar cells with aluminium oxide passivated rear side, Energy Procedia 77 (2015) 599–606, http://dx.doi.org/10.1016/j.egypro.2015.07.086.

[4] F. Kersten, P. Engelhart, H.C. Ploigt, F. Stenzel, K. Petter, T. Lindner, A. Szpeth, M. Bartzsch, A. Stekolnikov, M. Scherff, J. Heitmann, J.W. Muller, A new light induced volume degradation effect of mc-Si solar cells and modules, in: Proceedings of the 31st Eur. Photovolt. Sol. Energy Conf. Exhib., 2015, pp. 1822–1826.

[5] K.A. Ramspeck, S. Zimmermann, H. Nagel, A. Metz, Y. Gassenbauer, B. Birkmann, Seidl, Light induced degradation of rear passivated mc-Si solar cells, in: Proceedings of the 27th Eur. Photovolt. Sol. Energy Conf., 2012, pp. 861–865. ⟨http://dx.doi.org/10.1017/CBO9781107415324.004⟩.

[6] ITRPV, International Technology Roadmap for Semiconductors, 2016. ⟨papers2://publication/uuid/20F56C7C-3684-4039-B043-D3DE7C5293FA⟩.

[7] K. Petter, K. Hübener, F. Kersten, F. Fertig, B. Klöter, J. Müller, H.Q.C. Gmbh, Dependence of LeTID on brick height for different wafer suppliers with several resistivities and dopants, in: Proceedings of the 9th Int. Work. Cryst. Silicon Sol. Cell, Tempe Arizona, 2016.

[8] D. Chen, M. Kim, B.V. Stefani, B.J. Hallam, M.D. Abbott, C.E. Chan, R. Chen, D.N.R. Payne, N. Nampalli, A. Ciesla, T.H. Fung, K. Kim, S.R. Wenham, Evidence of an identical firing-activated carrier-induced defect in monocrystalline and multicrystalline silicon, Sol. Energy Mater. Sol. Cells 172 (2017) 293–300, http://dx.doi.org/10.1016/j.solmat.2017.08.003.

[9] F. Fertig, R. Lantzsch, A. Mohr, M. Schaper, M. Bartzsch, D. Wissen, F. Kersten, A. Mette, S. Peters, A. Eidner, J. Cieslak, K. Duncker, M. Junghänel, E. Jarzembowski, M. Kauert, B. Faulwetter-Quandt, D. Meißner, B. Reiche, S. Geißler, S. Hörnlein, C. Klenke, L. Niebergall, A. Schönmann, A. Weihrauch, F. Stenzel, A. Hofmann, T. Rudolph, A. Schwabedissen, M. Gundermann, M. Fischer, J. Müller, D.J. Jeong, Mass production of p-type Cz silicon solar cells approaching average stable conversion efficiencies of 22%, Energy Procedia 124 (2017) 338–345, http://dx.doi.org/10.1016/j.egypro.2017.09.308.

[10] D.N.R. Payne, C.E. Chan, B.J. Hallam, B. Hoex, M.D. Abbott, S.R. Wenham, D.M. Bagnall, Acceleration and mitigation of carrier-induced degradation in p-type multi-crystalline silicon, Phys. Status Solidi - Rapid Res. Lett. 10 (2016) 237–241, http://dx.doi.org/10.1002/pssr.201510437.

[11] W. Kwapil, T. Niewelt, M.C. Schubert, Kinetics of carrier-induced degradation at elevated temperature in multicrystalline silicon solar cells, Sol. Energy Mater. Sol. Cells 173 (2017) 80–84.

[12] T. Niewelt, M. Selinger, N.E. Grant, W. Kwapil, J.D. Murphy, M.C. Schubert, Light-induced activation and deactivation of bulk defects in boron-doped float-zone silicon, J. Appl. Phys. 185702 (2017) 1–8, http://dx.doi.org/10.1063/1.4983024.

[13] A. Herguth, G. Schubert, M. Kaes, G. Hahn, A new approach to prevent the negative impact of the metastable defect in boron doped CZ silicon solar cells, in: Proceedings of the 2006 IEEE 4th World Conf. Photovolt. Energy Conversion, WCPEC-4, 2007, pp. 940–943. ⟨http://dx.doi.org/10.1109/WCPEC.2006.279611⟩.

[14] B. Hallam, M. Abbott, N. Nampalli, P. Hamer, S. Wenham, B. Hallam, M. Abbott, N. Nampalli, P. Hamer, S. Wenham, Influence of the formation- and passivation rate of boron-oxygen defects for mitigating carrier-induced degradation in silicon within a hydrogen-based model, J. Appl. Phys. 119 (2016), http://dx.doi.org/10.1063/1.4941387.

[15] K. Krauß, A.A. Brand, F. Fertig, S. Rein, J. Nekarda, Fast regeneration processes to avoid light-induced degradation in multicrystalline silicon solar cells, IEEE J. Photovolt. 6 (2016) 1427–1431.

[16] J. Schmidt, K. Bothe, Structure and transformation of the metastable boron- and oxygen-related defect center in crystalline silicon, Phys. Rev. B 69 (2004) 1–8, http://dx.doi.org/10.1103/PhysRevB.69.024107.

[17] D. Bredemeier, D. Walter, J. Schmidt, Light-induced lifetime degradation in high-performance multicrystalline silicon: detailed kinetics of the defect activation, Sol. Energy Mater. Sol. Cells 173 (2017) 2–5, http://dx.doi.org/10.1016/j.solmat.2017.08.007.

[18] T. Luka, S. Großer, C. Hagendorf, K. Ramspeck, M. Turek, Intra-grain versus grain boundary degradation due to illumination and annealing behavior of multi-crystalline solar cells, Sol. Energy Mater. Sol. Cells 158 (2016) 43–49, http://dx.doi.org/10.1016/j.solmat.2016.05.061.

[19] M.A. Jensen, A.E. Morishige, J. Hofstetter, D.B. Needleman, Evolution of LeTID defects in p-type multicrystalline silicon during degradation and regeneration, IEEE J. Photovolt. (2017) 1–8.

[20] C. Chan, T.H. Fung, M. Abbott, D. Payne, A. Wenham, B. Hallam, R. Chen, S. Wenham, Modulation of carrier-induced defect kinetics in multi-crystalline silicon PERC cells through dark annealing, Phys. Status Solidi (RRL)-Rapid Res. Lett. 1 (2017), http://dx.doi.org/10.1002/solr.201600028.

[21] W. Shockley, W.T. Read, Statistics of the recombination of holes and electrons, Phys. Rev. 87 (1952) 835–842.

[22] J. Schmidt, A.G. Aberle, R. Hezel, Investigation of carrier lifetime instabilities, in: Proceedings of the Photovolt. Spec. Conf., Conf. Rec. Twenty-Sixth IEEE, IEEE, n.d, pp. 13–18.

[23] T.H. Fung, C.E. Chan, B.J. Hallam, D.N.R. Payne, M.D. Abbott, S.R. Wenham, Impact of annealing on the formation and mitigation of carrier-induced defects in multi-crystalline silicon, Energy Procedia 124 (2017) 726–733.

[24] A. Herguth, G. Hahn, Kinetics of the boron-oxygen related defect in theory and experiment, J. Appl. Phys. 108 (2010) 1–7, http://dx.doi.org/10.1063/1.3517155.

[25] B. Hallam, M. Abbott, T. Nærland, S. Wenham, Fast and slow lifetime degradation in boron-doped Czochralski silicon described by a single defect, Phys. Status Solidi - Rapid Res. Lett. 524 (2016) 520–524, http://dx.doi.org/10.1002/pssr.201600096.

[26] M. Kim, M. Abbott, N. Nampalli, S. Wenham, B. Stefani, B. Hallam, Modulating the extent of fast and slow boron-oxygen related degradation in Czochralski silicon by thermal annealing: evidence of a single defect, J. Appl. Phys. 53106 (2017) 1–10, http://dx.doi.org/10.1063/1.4975685.

[27] Z. Hameiri, N. Borojevic, L. Mai, N. Nandakumar, K. Kim, S. Winderbaum, Should the refractive index at 633 nm be used to characterize silicon nitride films?, in: Proceedings of the 43rd IEEE Photovolt. Spec. Conf., 2016, pp. 2900–2904.

[28] H. Nagel, C. Berge, A.G. Aberle, H. Nagel, C. Berge, A.G. Aberle, Generalized analysis of quasi-steady-state and quasi-transient measurements of carrier lifetimes in semiconductors, J. Appl. Phys. 86 (1999) 6218–6221, http://dx.doi.org/10.1063/1.371633.

[29] R.A. Sinton, A. Cuevas, M. Stuckings, Quasi-steady-state photoconductance, a new method for solar cell material and device characterization, in: Proceedings of the 25th IEEE Photovolt. Spec. Conf., 1996, pp. 457–460.

[30] A. Richter, S.W. Glunz, F. Werner, J. Schmidt, A. Cuevas, Improved quantitative description of Auger recombination in crystalline silicon, Phys. Rev. B 165202 (2012) 1–14, http://dx.doi.org/10.1103/PhysRevB.86.165202.

[31] N. Nampalli, T.H. Fung, S. Wenham, B. Hallam, M. Abbott, M. Abbott, Statistical analysis of recombination properties of the boron-oxygen defect in p-type Czochralski silicon, Front. Energy 11 (2017) 4–22, http://dx.doi.org/10.1007/s11708-016-0442-6.

[32] D. Sperber, A. Graf, D. Skorka, A. Herguth, G. Hahn, degradation of surface passivation on crystalline silicon and its impact on light induced degradation experiments, IEEE J. Photovolt. Prepr. (2017), http://dx.doi.org/10.1109/JPHOTOV.2017.2755072.

[33] A.E. Morishige, M.A. Jensen, D.B. Needleman, K. Nakayashiki, J. Hofstetter, T.A. Li, T. Buonassisi, Lifetime spectroscopy investigation of light-induced degradation in p-type multicrystalline silicon PERC, IEEE J. Photovolt. 6 (2016) 1466–1472.

[34] D. Bredemeier, D. Walter, S. Herlufsen, J. Schmidt, D. Bredemeier, D. Walter, S. Herlufsen, Lifetime degradation and regeneration in multicrystalline silicon under illumination at elevated temperature, AIP Adv. 35119 (2017), http://dx.doi.org/10.1063/1.4944839.

[35] C.E. Chan, D.N.R. Payne, B.J. Hallam, M.D. Abbott, T.H. Fung, A.M. Wenham, B.S. Tjahjono, S.R. Wenham, Rapid stabilization of high-performance multicrystalline p-type silicon PERC cells, IEEE J. Photovolt. 6 (2016) 1473–1479.

[36] K. Nakayashiki, J. Hofstetter, A.E. Morishige, T.A. Li, D.B. Needleman, M.A. Jensen, T. Buonassisi, Engineering solutions and root-cause analysis for light-induced degradation in p-type multicrystalline silicon PERC modules, IEEE J. Photovolt. 6 (2016) 860–868.

[37] W. Kwapil, Understanding the light-induced degradation at elevated temperatures: similarities between multicrystalline and floatzone p-type silicon, in: EUPVSEC Plenary Talk, 2017.

[38] V.V. Voronkov, R. Falster, Formation, dissociation, and diffusion of various hydrogen dimers in silicon, Phys. Status Solidi 6 (2017) 254, http://dx.doi.org/10.1002/pssb.201600779.

[39] R.E. Pritchard, J.H. Tucker, R.C. Newman, E.C. Lightowlers, Hydrogen molecules in boron-doped crystalline silicon, Semicond. Sci. Technol. 14 (1999) 77–80.

[40] M.J. Binns, S.A. McQuaid, R.C. Newman, E.C. Lightowlers, Hydrogen solubility in silicon and hydrogen defects present after quenching, Semicond. Sci. Technol. 8 (1993).

[41] A. Ciesla, Advanced laser processing for next-generation silicon wafer solar cells, 2017.

[42] T. Zundel, J. Weber, Boron reactivation kinetics in hydrogenated silicon after annealing in the dark or under illumination, Phys. Rev. B 43 (1991) 4361–4372.

[43] C.H. Seager, R.A. Anderson, Two-step debonding of hydrogen from boron acceptors in silicon, Appl. Phys. Lett. 59 (1991) 585, http://dx.doi.org/10.1063/1.105394.

[44] S.A. Mcquaid, M.J. Binns, R.C. Newman, E.C. Lightowlers, J.B. Clegg, Solubility of hydrogen in silicon at 1300 °C, Appl. Phys. Lett. 1612 (1993), http://dx.doi.org/10.1063/1.108602.

[45] W.B. Jackson, N.M. Johnson, C.C. Tsai, I.-W. Wu, a. Chiang, D. Smith, Hydrogen diffusion in polycrystalline silicon thin films, Appl. Phys. Lett. 61 (1992) 1670, http://dx.doi.org/10.1063/1.108446.

[46] T. Luka, M. Turek, S. Großer, C. Hagendorf, Light induced degradation – defect gettering at Grain boundaries, in: Proceedings of the 33rd Eur. Photovolt. Slar Energy Conf. Exhib., 2017, pp. 1143–1146.

[47] D. Bredemeier, D.C. Walter, J. Schmidt, Possible Candidates for Impurities in mc-Si Wafers Responsible for Light-Induced Lifetime Degradation and Regeneration, Sol. Rrl. 1700159 (2018) 1–5, http://dx.doi.org/10.1002/solr.201700159.

[48] S. Wilking, C. Beckh, S. Ebert, A. Herguth, G. Hahn, Influence of bound hydrogen states on BO-regeneration kinetics and consequences for high-speed regeneration processes, Sol. Energy Mater. Sol. Cells 131 (2014) 2–8, http://dx.doi.org/10.1016/j.solmat.2014.06.027.